METTL14-mediated epitranscriptome modification of MN1 mRNA promote tumorigenicity and all-trans-retinoic acid resistance in osteosarcoma

Hong-Bo Li,[a,b,1] Gang Huang,[a,b,1] Jian Tu,[a,b,1] Dong-Ming Lv,[a,b] Qing-Lin Jin,[a,b] Jun-Kai Chen,[a,b] Yu-Tong Zou,[a,b] Dung-Fang Lee,[c] Jing-Nan Shen,[a,b]* and Xian-Biao Xie[a,b]*

[a]Department of Musculoskeletal Oncology, The First Affiliated Hospital of Sun Yat-sen University, Guangzhou 510080, China
[b]Guangdong Provincial Key Laboratory of Orthopedics and Traumatology, The First Affiliated Hospital of Sun Yat-sen University, Guangzhou 510080, China
[c]Department of Integrative Biology & Pharmacology, McGovern Medical School, University of Texas Health Science Center at Houston, TX 77030-1501, US

eBioMedicine 2022;82: 104142
Published online xxx
https://doi.org/10.1016/j.ebiom.2022.104142

Summary

Background Osteosarcoma (OS) is the most common primary malignant bone tumor in adolescents. The molecular mechanism behind OS progression and metastasis remains poorly understood, which limits the effectiveness of current therapies. RNA N^6-methyladenosine (m^6A) modification plays a critical role in influencing RNA fate. However, the biological significance of m^6A modification and its potential regulatory mechanisms in the development of OS remain unclear.

Methods Liquid chromatography-tandem mass spectrometry (LC-MS/MS), dot blotting, and colorimetric ELISA were used to detect m^6A levels. Western blotting, quantitative real-time PCR (RT-qPCR) and immunohistochemistry (IHC) were used to investigate METTL14 expression levels. Methylated RNA immunoprecipitation sequencing (MeRIP-seq) and transcriptomic RNA sequencing (RNA-seq) were used to screen the target genes of METTL14. RNA pull-down and RNA immunoprecipitation (RIP) assays were conducted to explore the specific binding of target genes and relevant m^6A "readers". RNA stability and polysome analysis assays were used to detect the half-lives and translation efficiencies of the downstream genes of METTL14. IHC and clinical data were applied to explore the clinical correlations of METTL14 and its downstream target genes with the prognosis of OS.

Findings We observed the abundance of m^6A modifications in OS and revealed that METTL14 plays an oncogenic role in facilitating OS progression. MeRIP-seq and RNA-seq revealed that MN1 is a downstream gene of METTL14. MN1 contributes to tumor progression and all-trans-retinoic acid (ATRA) chemotherapy resistance in OS. Mechanistically, MN1 is methylated by METTL14, specifically in the coding sequence (CDS) regions, and this modification is recognized by the specific m^6A reader insulin-like growth factor 2 mRNA binding protein 2 (IGF2BP2) to prevent MN1 mRNA degradation and promote it translation efficiency. IHC showed that MN1 expression was positively correlated with METTL14 and IGF2BP2 expression in OS tissues. The METTL14-IGF2BP2-MN1 panel demonstrated more promising prognostic value for OS patients than any of these molecules individually.

Interpretation Our study revealed that METTL14 contributes to OS progression and ATRA resistance as an m^6A RNA methylase by regulating the stability and translation efficiency of MN1 and thus provides both an underlying biomarker panel for prognosis prediction in OS patients.

Funding This work was supported by the National Natural Science Foundation of China (Grants 81972510 and 81772864).

Keywords: Osteosarcoma; METTL14; m^6A modification; Lung metastasis

*Corresponding authors at: Department of Musculoskeletal Oncology, The First Affiliated Hospital of Sun Yat-sen University, No.58, Zhongshan Rd.2, Guangzhou 510080, China.
E-mail addresses: shenjn@mail.sysu.edu.cn (J.-N. Shen), xiexbiao@mail.sysu.edu.cn (X.-B. Xie).

[1] H. Li, G. Huang, J. Tu contributed equally to this work.

Research in context

Evidence before this study

The m^{6}A modification regulates RNA biological functions via m^{6}A methyltransferases, demethylases, and readers. METTL14, a key component of the m^{6}A methyltransferase complex, can stabilize the structure of METTL3, enhance the enzyme activity of METTL3 by binding with RNA, and affect the overall m^{6}A level. However, the biological significance of m^{6}A modification and its potential regulatory mechanisms in the development of OS remain unclear. METTL14 plays an essential regulatory role in the occurrence and development of malignant tumors. Although recent study has shown that METTL14 act as a tumor suppressor gene in osteosarcoma, the studies of METTL14 in osteosarcoma were still limited, the molecular mechanism of METTL14 in osteosarcoma is still unclear.

Added value of this study

We revealed the critical role of METTL14 in OS progression and ATRA resistance and showed that this role is dependent on its m^{6}A catalytic activity. Mechanistically, METTL14 mediates m^{6}A demethylation of MN1 mRNA to promote its stability and translation via an IGF2BP2-dependent mechanism in OS.

Implications of all the available evidence

Our work suggests that METTL14 might be a potential prognostic predictor and therapeutic target for OS patients and provides an essential molecular foundation for ATRA treatment against OS.

Introduction

Osteosarcoma (OS) is the most common primary malignant bone tumor in children and adolescents and accounts for 55% of all primary malignant tumors of bone.[1] In the last two decades, the 5-year survival rate has increased to 60–70% in patients with localized tumors, but the 5-year survival rate for patients with recurrent or metastatic OS is less than 25%.[2,3] Surgery and intensive adjuvant chemotherapy are the typical treatments for OS patients.[4] However, the survival rate of OS patients with surgical treatment alone is approximately 15–17%, and standard adjuvant/neoadjuvant chemotherapy does not have remarkable antineoplastic effects in some OS patients.[5,6] In addition, the molecular mechanism underlying OS progression and metastasis remains poorly understood.

The latest epitranscriptome research reveals that RNA N^6-methyladenosine (m^{6}A) modification, which refers to the methylation of the N^6 position on adenosine, is the most abundant known intrinsic chemical modification of mRNA in eukaryotic cells.[7] The m^{6}A modification plays a critical role in influencing RNA fate, including precursor mRNA maturation, translation and stability.[8] Accumulating evidence has shown that mRNA m^{6}A modification plays a critical role in regulating malignant tumor occurrence and development.[9–11] The m^{6}A modification in mammalian cells can be conferred by the m^{6}A methyltransferases METTL3, METTL14, and WTAP, called "writers", and removed by the m^{6}A demethylases FTO and ALKBH5, called "erasers". In addition, specific m^{6}A binding proteins, including IGF2BP1/2/3 and the YTH family proteins, have been identified as m^{6}A "readers" that modulate the fate of methylated mRNAs to mediate downstream effects.[12–15] Recent studies have found that mRNA m^{6}A modification is vitally important in leukemia,[16] endometrial cancer,[17] hepatocellular carcinoma,[18,19] gastric cancer,[20] and other tumors. However, the biological significance of m^{6}A modification and its potential regulatory mechanisms in the development of OS remain unclear.

Meningioma 1 (MN1) is reported to be a fusion partner of TEL, an ETS transcription factor, in patients with acute myeloid leukemia (AML) or myelodysplastic syndrome containing the translocation t(12;22)(p13;q11),[21] which is a unique oncogene in hematopoiesis that both promotes proliferation/self-renewal and blocks differentiation.[22] Interestingly, MN1 locates in retinoic acid response elements (RAREs) and has a dominant-negative effect on receptor/retinoic X receptor (RAR/RXR) -mediated transcription.[23] High expression of MN1 indicates a poor prognosis and induces resistance to all-trans-retinoic acid (ATRA) in AML patients.[24] However, the functions and tumor-promoting ability of MN1 and its relationship to ATRA therapy in OS are still unexplored.

Numerous experiments and clinical trials have confirmed that ATRA and its derivatives are effective and promising drug used for treating acute promyelocytic leukemia (APL) and various other tumor types, including neuroblastoma, melanoma, and breast cancer.[25] ATRA has been widely used in the treatment of APL for decades and has revolutionized the outcomes of patients with APL. Some studies have reported that ATRA can inhibit proliferation and metastasis in OS.[26–30] However, the clinical application of ATRA for OS treatment has no advances in the past two decades.

In this study, we observed the abundance of m^{6}A modifications in OS and revealed that METTL14 plays an oncogenic role in facilitating OS progression. Then, we identified MN1 as a downstream target of METTL14, whose stability and translation were regulated by the specific m^{6}A reader insulin-like growth factor 2 mRNA binding protein 2 (IGF2BP2), contributing to tumor progression and ATRA chemotherapy resistance in OS. Further, we revealed that METTL14-IGF2BP2-MN1 is an underlying promising biomarker panel for prognosis prediction in OS patients.

Methods

Human samples and cell lines

The study was approved by the Ethics Committee of The First Affiliated Hospital of Sun Yat-sen University, Guangzhou (Reference number: [2021] 755). All the patients signed an informed consent form. A total of 50 tumor tissues and adjacent normal tissues were used for quantitative real-time PCR (RT-qPCR), m^6A levels and western blot detection. Another 70 tumor tissues were used for immunohistochemistry (IHC) analysis.

The BMSC (RRID: CVCL_A9JT), HL60 (RRID: CVCL_0002) and human OS cell lines SJSA-1 (RRID: CVCL_1697), U2OS (RRID: CVCL_0042), HOS (RRID: CVCL_0312), MNNG/HOS (RRID: CVCL_0439), 143B (RRID: CVCL_2270) and MG-63 (RRID: CVCL_0426) were obtained from ATCC. U2OS/MTX300 cells, a methotrexate-resistant derivative of the U2OS human OS cell line, were kindly provided by Dr. M. Serra (Instituti Ortopedici Rizzoli, Bologna, Italy). ZOS and ZOS-M, syngeneic human OS cell lines derived from a primary tumor and metastatic lesion of the same patient, were described previously.[31] All of the cells used were authenticated and free of mycoplasma contamination before the experiments, and were performed and cultured according to the instructions from American Type Culture Collection (ATCC). The HL-60 was cultured in IMDM medium (Gibco) containing L-glutamine (Corning), other cell lines were cultured in DMEM (Gibco) supplemented with 10% fetal bovine serum (Invitrogen) at 37°C and 5% CO_2.

RNA m^6A methylation assay

Total RNA was isolated using TRIzol (Invitrogen, USA) according to the manufacturer's instructions. RNA quality was analyzed by NanoDrop. The change in m^6A level relative to the total mRNA level was measured using the m^6A RNA Methylation Quantification Kit (Colorimetric) (ab185912; Abcam) following the manufacturer's protocol. Each sample was analyzed using 200 ng of RNA. The m^6A levels were quantified colorimetrically by reading the absorbance of each well at a wavelength of 450 nm, and then calculations were performed based on the standard curve.

RNA m^6A dot blot assay

The m^6A dot blot assay was conducted as previously described. Briefly, the indicated amount of total RNA was denatured in incubation buffer at a 1:3 ratio (65.7% formamide, 7.77% formaldehyde and 1.33 × MOPS) at 65°C for 5 min, followed by chilling on ice and mixing with 20 × SSC buffer at a 1:1 ratio. RNA samples were transferred to an Amersham Hybond-N+ membrane (GE Healthcare) with a Bio-Dot Apparatus (Bio-Rad) and auto-crosslinked 3 times with the auto-crosslinking mode. After UV crosslinking, the membrane was stained in 0.3 M sodium acetate with 0.02% methylene blue (MB). Then, the membrane was washed with 1 × PBST buffer, blocked in 5% nonfat milk in PBST for 1 h at room temperature and incubated with anti-m^6A antibody (202003, 1:1,000; Synaptic Systems) overnight at 4°C. The membrane was washed according to the standard protocol. After incubation with horseradish peroxidase-conjugated anti-rabbit IgG secondary antibody (Santa Cruz Biotechnology), the membrane was visualized using Amersham ECL Prime Western Blotting Detection Reagent (GE Healthcare).

MeRIP-seq

MeRIP was conducted as previously published with minor revisions.[32] Total RNA was evaluated with a NanoDrop ND-1000, and intact mRNA was isolated using an Arraystar Seq-Star™ poly(A) mRNA Isolation Kit (Arraystar, MD, USA) according to the manufacturer's instructions. Purified mRNA was randomly fragmented into approximately 100-nt fragments by incubation in fragmentation buffer. Fragmented mRNA was immunoprecipitated with anti-m^6A antibody (202,003, Synaptic Systems), and 1/10 of the fragmented mRNA was kept as input for further RNA sequencing. RNA-seq libraries were prepared using the KAPA Stranded mRNA-seq Kit (Illumina, CA, USA). The methylated RNA was purified and sequenced on an Illumina HiSeq 4000 platform by Aksomics (Shanghai, China).

LC-MS/MS for determination of the m^6A/A ratio

Double selected polyadenylated (poly(A)) mRNA was digested by nuclease P1 (1 U, Sigma) in 25 ml of buffer containing 20 mM NH_4OAc (pH=5.3) at 37°C for 1 h, followed by an additional incubation with the addition of freshly made NH_4HCO_3 (1 M, 3 ml) and alkaline phosphatase (1 U, Sigma) at 37°C for 4 h. The samples were diluted to 50 ml and filtered (0.22-μm pore size, 4 mm diameter, Millipore), and 5 ml of the solution was injected for LC-MS/MS. Nucleosides were separated by reversed-phase ultra-performance liquid chromatography on a C18 column with online mass spectrometry detection by an Agilent 6410 QQQ triple-quadrupole LC mass spectrometer in positive electrospray ionization mode. The nucleosides were quantified by using retention time and nucleoside to base ion mass transitions of 282.1 to 150.1 (m^6A), 268 to 136 (A), 284 to 152 (G), 245 to 113.1 (U), and 244 to 112 (C). Quantification was performed in comparison with the standard curve obtained from pure nucleoside standards run with the same batch of samples. The m^6A level was calculated as the ratio of m^6A to A based on the calibrated concentrations.

Western blot assay

Equal amounts of protein lysates were resolved on SDS-PAGE gels and then transferred to PVDF membranes (Millipore). The membranes were blocked in 5% nonfat

dry milk at room temperature for 1 h and then incubated with a primary antibody at 4°C overnight. Next, membranes were incubated with a secondary antibody for 1 h at room temperature. The immunoreactive signals were visualized by an enhanced chemiluminescence kit (Amersham Biosciences, Uppsala, Sweden).

The antibodies used for IHC and western blotting assays were as follows: METTL14 (Sigma, HPA038002, AB_10672401), MN1 (Proteintech, 24697-1-AP, AB_2879678), SOX2 (CST, #3579, AB_2195767), OCT4 (CST, #2750, AB_823583), CD133 (CST, #64326, AB_2721172), MMP-2 (CST, #40994, AB_2799191), IGF2BP2 (Proteintech, 11601-1-AP, AB_2122672), IGF2BP1 (Proteintech, 22803-1-AP, AB_2879173), IGF2BP3 (Proteintech, 14642-1-AP, AB_2122782), YTHDF1 (Proteintech, 17479-1-AP, AB_2217473), YTHDF2 (Proteintech, 24744-1-AP, AB_2687435), GAPDH (Proteintech, 10494-1-AP, AB_2263076), and Ki-67 (CST, #9449, AB_2715512).

Lentiviral transduction for stable cell lines

The lentiviruses packaging METTL14 shRNA (targeting sequences: #sh32: GGTTACAGAAGATGTGAAGAT, #sh33: GCTAATGTTGACATTGACTTA) and MN1 shRNA (targeting sequences: #sha: GGCATCATGTCTAACTCTACC, #shb: GCGCAATTCGAGTATCCCATC) were purchased from GeneCopoeia (Shanghai, China). Transfection experiments were performed with Lipofectamine 3000 (Invitrogen). To establish stable METTL14 and MN1 knockdown cell lines, OS cells were transduced by lentiviruses and selected with puromycin (2 μg/ml, InvivoGen) after 3 days production. For the MN1 rescue experiment, MN1-CDS were cloned to pcDNA3.1 vector, and then the empty vector or the MN1-CDS were transduced to the METTL14 knockdown and scramble OS cells, respectively.

RNA extraction and quantitative real-time PCR (RT-qPCR) analysis

Total RNA was extracted with TRIzol reagent (Invitrogen, Carlsbad, USA), and cDNA was generated using the PrimeScript RT Reagent Kit (Takara) according to the manufacturer's instructions. RT-PCR was carried out using SYBR Green SuperMix (Roche, Basel, Switzerland) and an ABI7900HT Fast Real-Time PCR system (Applied Biosystems, CA, USA). GAPDH was used as an internal control. The primer sequences are listed in Supplementary Table S1.

Cell proliferation/growth

Cell proliferation/growth was assessed by Cell Counting Kit-8 (CCK-8) assays following the manufacturer's instructions. Briefly, OS cells were seeded in triplicate in 96-well plates at a density of 2,000−10,000 cells/200 μL. Then, dye solution was added at the indicated time points, and the plates were incubated at 37°C for 3−4 h before the absorbance was detected at 450 nm.

Cell sphere formation and colony formation assay

A total of 2×10^3 cells were plated in 96-well ultralow attachment plates (7007, Corning) with serum-free DMEM-F12 medium including 20 ng/ml epidermal growth factor (EGF) (236-EG, RD), 20 ng/ml basic fibroblast growth factor (bFGF) (233-FB, RD) and 20 ng/ml N2 medium (2229-N2, RD). After 7 days, the spheres with diameters greater than 50 μm in each well were counted under a microscope. A volume of 2 mL of complete medium containing 1000 OS cells was placed in each well of a six-well plate. In the ATRA experiment, 2000 plated cells were incubated with DMSO or ATRA for 48 h. Colonies containing >50 cells were counted after 10 days by staining with crystal violet. Data are presented as the mean ± SD from three independent experiments in triplicate chambers.

Wound healing and Transwell assays

Wound healing assays were performed using six-well plates, and cells were seeded and cultured in almost 90% confluent monolayers. Then, the cells were scratched using a sterile pipette tip and treated in FBS-free medium. The cell migration distances were measured under a microscope. Transwell assays were performed using a 24-well Transwell system (Corning) with polycarbonate filters (8-μm pores, Corning) with or without a precoating of extracellular matrix coating (BD Biosciences), respectively, according to the manufacturer's instructions. Briefly, 200 μL of suspensions with 5×10^4 OS cells in serum-free DMEM were seeded in the upper chambers of 24-well plates, and 500 μL of DMEM containing 20% FBS was added to the bottom chambers. After 24 h of incubation at 37°C, the cells in the Transwell system were stained with 0.25% crystal violet. The cells remaining in the upper Transwell chamber were removed, and those that migrated to the lower chamber were photographed and counted. The data are presented as the mean ± SD from three independent experiments in triplicate chambers.

ALDEFLUOR assay

The ALDEFLUOR assay was performed with an ALDEFLUOR kit (Stem Cell Technologies, Vancouver, BC, Canada) to determine the ALDH activity of OS cells by fluorescence-activated cell sorting according to the manufacturer's instructions. The experiments were performed in triplicate.

RNA immunoprecipitation (RIP) assays

RIP assays were performed using the Magna RIP RNA-Binding Protein Immunoprecipitation Kit (17-700,

Millipore) according to the manufacturer's instructions. Briefly, Protein-A/G beads (Roche, USA) and 5 μg of specific antibodies were incubated with cell lysates from U2OS and 143B cells overnight at 4°C. Then, the immune complexes were washed six times with washing buffer and incubated with proteinase K digestion buffer. Next, total RNA was extracted and assessed by qPCR and normalized to the input.

RNA pull-down assays

The RNA pull-down assays were performed with the Pierce Magnetic RNA-Protein Pull-Down Kit (Thermo Fisher Scientific, 20164) according to the manufacturer's instructions. Biotinylated RNAs were synthesized with the T7 Transcription Kit (Thermo Fisher Scientific). Up to 50 pmol of biotinylated RNAs and 50 μL of magnetic beads were used for each sample. After incubation and three washes, the proteins in the RNA-protein complex were identified by western blotting, silver staining or mass spectrometry analysis.

m^{6}A mutation assays

The potential m^{6}A sites for RNA were predicted by an online tool, SRAMP (http://www.cuilab.cn/sramp/). The m^{6}A motif-depleted mRNA regions were cloned into pcDNA3.1 for the RNA pull-down assay. The specific sequences are shown in Supplementary Table S2.

RNA stability assays

U2OS and 143B cells were seeded in 6-well plates overnight, treated with Act D (HY-17559, MCE) at a final concentration of 5 μg/mL for 0, 3, or 6 h and collected. Total RNA was extracted using TRIzol reagent (Invitrogen, Carlsbad, USA) and analyzed by RT-PCR. The half-life of mRNA was estimated according to a previously published paper.[33]

Polysome profiling

Polysome profiling followed the reported protocols with the following modifications.[12,34] Briefly, 143B cells were infected with lentiviral shRNA targeting METTL14 or transfected with IGF2BP2 short interfering (siRNA). Before collection, cycloheximide (CHX) was added to the culture media at 100 μg/ml for 7 min. The lysis buffer was formulated as 20 mM HEPES, pH 7.6, 5 mM $MgCl_2$, 100 mM KCl, 100 μg/ml cycloheximide, and 1% Triton X-100, with freshly added 1:100 protease inhibitor (Roche) and 40 U/ml SUPERasin (Ambion). Then, the sample was fractionated into 24 fractions (0.5 mL per fraction) and analyzed with a Gilson FC203B fraction collector (Mandel Scientific, Guelph, Canada) and a Gradient Station (BioCamp) equipped with an ECONOUV monitor (BioRad, Hercules, CA). RNA was purified from fractions 5–18 and subjected to qPCR analysis of the MN1 transcript.

Animal models

All animal experiments were approved by the Institutional Review Board of The First Affiliated Hospital of Sun Yat-sen University and were performed according to established guidelines for the Use and Care of Laboratory Animals (Reference number: [2018] 236). All female BALB/c nude mice (4 to 5 weeks old) were purchased from GemPharmatech Co. Ltd. All the mice were randomly divided into each group and five mice were fed in each cage. After the mice were anesthetized with isoflurane, 1×10^6 wild-type cells or plasmid-transfected cells in a 20-μL suspension were inserted into the proximal tibia through the cortex of the anterior tuberosity using a 30-gauge needle (n=6 per group).

In the lung metastasis model, 1×10^6 cells suspended in 100 μl PBS were injected intravenously into the tail vein (n=6 per group). Six weeks later, the mice were sacrificed, and the lungs were excised, imaged and paraffin embedded. Subsequently, the numbers of metastatic nodules in the lungs were carefully examined.

For the study of ATRA, the mice were randomly divided into two groups after approximately 14 days when the tumor volumes reached approximately 200 mm^3. The mice were treated with 10% DMSO or 25 mg/kg ATRA every 3 days by intraperitoneal (i.p.) injection (n=6 per group). The mice were monitored every 3 days over 3 weeks. As the tumors grew as almost spherical ellipsoids, the size of tumors was measured in two perpendicular dimensions (D1, D2). The tumor volume was calculated using the formula $V=4/3\pi\ [1/4\ (D1 + D2)]^2$, as described previously.[35] Thirty-two days after cell injection, the mice were euthanized.

Statistical analysis

All results were derived from at least three independent experiments, and data from one representative experiment are shown. The data are presented as the mean ± standard deviation (SD). The statistical significance of differences was evaluated by two-tailed Student's t test, one-way ANOVA or χ^2 test. Overall survival was assessed with the Kaplan–Meier method and compared by the log-rank test. Differences with p values < 0.05 were considered statistically significant. All statistical analyses were carried out using R or GraphPad Prism (version 6.0).

Role of funding source

Funders of the study did not have any role in study design, data collection, data analysis, data interpretation, or writing of the report.

Results

METTL14 is highly expressed in clinical osteosarcoma specimens and correlates with poor prognosis

To elucidate the functional roles of m^{6}A modification in osteosarcomagenesis, we first examined the global m^{6}A

levels in OS tissues and paired normal muscular tissues. Quantification of m^6A RNA methylation by liquid chromatography-tandem mass spectrometry (LC-MS/MS) indicates m^6A RNA modification levels are significantly elevated in 3 paired OS tissues compared with normal control samples (Figure 1(a)). The results were further validated by colorimetric ELISA in 50 paired OS tissues and dot blot assay in 3 paired OS tissues (Figure 1 (b) and (c)). In addition, the m^6A RNA modification levels were significantly elevated in OS tissues from patients with lung metastasis compared with tissues from those without lung metastasis (Figure 1(d)), indicating the direct correlation between m^6A RNA modification and aggressive stage of OS. To elucidate the underlying mechanism of m^6A upregulation, we then measured the expression levels of m^6A writers (METTL3, METTL14, and WTAP) and m^6A erasers (FTO and ALKBH5) in 50 OS tissues and paired normal tissues. Surprisingly, the results showed that among these m^6A factors, METTL14 showed the highest upregulation in tumor samples (Figure 1(e)). Consistently, immunoblotting confirmed elevated METTL14 protein levels in OS samples compared to adjacent normal tissues (Figure 1(f)). Moreover, the increase of METTL14 protein was observed in numerous OS cell lines compared to bone marrow stem cells (BMSCs) (Figure 1(g)). To investigate the clinical implication of METTL14 in OS, we performed immunohistochemistry (IHC) staining to examine METTL14 expression in clinical OS specimens (n=70) (Figure 1(h)) and found that high METTL14 expression in the OS cohort is significantly correlated with clinicopathological features, such as lung metastasis. In particular, high METTL14 expression was closely associated with a high rate of pulmonary metastasis in OS (Supplemental Table S3). Moreover, OS patients with high METTL14 expression had worse overall survival and lung metastasis-free survival (LMFS) times than other patients through Kaplan-Meier analysis (Figure 1(i)). Taken together, these results reveal that m^6A modification levels and METTL14 expression are increased in OS and suggest that METTL14 is a prognostic factor for OS patients.

METTL14 promotes OS proliferation and metastasis in vitro and in vivo

To investigate the functional roles of METTL14 in osteosarcomagenesis, we established stable METTL14 knockdown models in U2OS and 143B cells with two independent short hairpin RNA (shRNA) sequences (shMETTL14 #32 and #33) (Figure 2(a)). Dot blot assay and colorimetric ELISA indicated the mRNA m^6A methylation levels are dramatically reduced in METTL14-depleted cells (Figure 2(b) and (c)). Knockdown of METTL14 significantly suppressed the cell proliferation, colony formation, wound healing ability, migration, and invasion abilities of both U2OS and 143B OS cells (Figure 2(d-f) and Figure S1(a)), suggesting the tumorigenic role of METTL14 in OS. Since METTL14 functions as a key m^6A methyltransferase, we then examined whether these functions of METTL14-mediated tumorigenic abilities are dependent on its m^6A catalytic activity. Plasmids expressing wild-type METTL14 and its catalytic dead mutant (R298P) were constructed and transfected into OS cells (Figure 2 (g) and (h)). *In vitro* studies of cellular effects of METTL14 and METTL14-R298P suggested that in comparison with vector controls METTL14 but not METTL14-R298P promotes OS proliferation and migration (Figure 2(i) and (j)). WT-METTL14 could rescue the proliferation abilities in osteosarcoma cells (Figure S1 (b)). Furthermore, in vivo xenograft studies using orthotopic animal models revealed knockdown of METTL14 significantly inhibits 143B tumor growth *in vivo*, as reflected by the differences in xenograft tumor size and weight between knockdown and vector control cell-derived tumors (Figure 2(k-n)). Knockdown of METTL14 also decreased the expression of MMP-2 in xenograft tumor (Figure S1(c)). To determine the roles of METTL14 in OS lung metastasis *in vivo*, 143B cells with METTL14 knockdown and the corresponding control cells were injected intravenously into nude mice. After six weeks, we observed that knockdown of METTL14 significantly inhibited OS lung metastasis, as evidenced by decrease in the number and size of metastatic lung lesions in the knockdown group versus the control group (Figure 2(o)). In summary, these data suggest that METTL14 promotes OS proliferation and metastasis *in vitro* and *in vivo* and METTL14-mediated tumorigenic function is dependent on its m^6A catalytic activity.

METTL14 maintains the stemness of OS cells

The m^6A modification has been reported to regulate cancer stemness in several malignancies.[36–39] To determine whether METTL14 plays a crucial role in the stemness of OS, we first cultured U2OS and 143B cells in cell sphere formation medium to collect sarcospheres, sphere-forming cell subsets with cancer stem cell properties. Quantitative RT-PCR (qRT-PCR) and western blotting revealed cancer stemness markers such as CD133, SOX2, and OCT4 are obviously elevated in sarcospheres compared to their parental cells (Figure 3(a) Figure S2(a)). Moreover, the m^6A levels and METTL14 levels were also significantly increased in sarcospheres compared to their parental cells (Figure 3(b) and (c)). Depletion of METTL14 lead to downregulation of CD133, SOX2, and OCT4 expression in U2OS and 143B cells (Figure 3(d)). A decrease in sphere number and size and a marked reduction in ALDH activity were also observed in METTL14 knockdown (METTL14-KD) U2OS and 143B cells compared with the control cells (Figure 3(e) and (f)). These results together indicate that increased m^6A modification and METTL14 expression promote OS cell stemness.

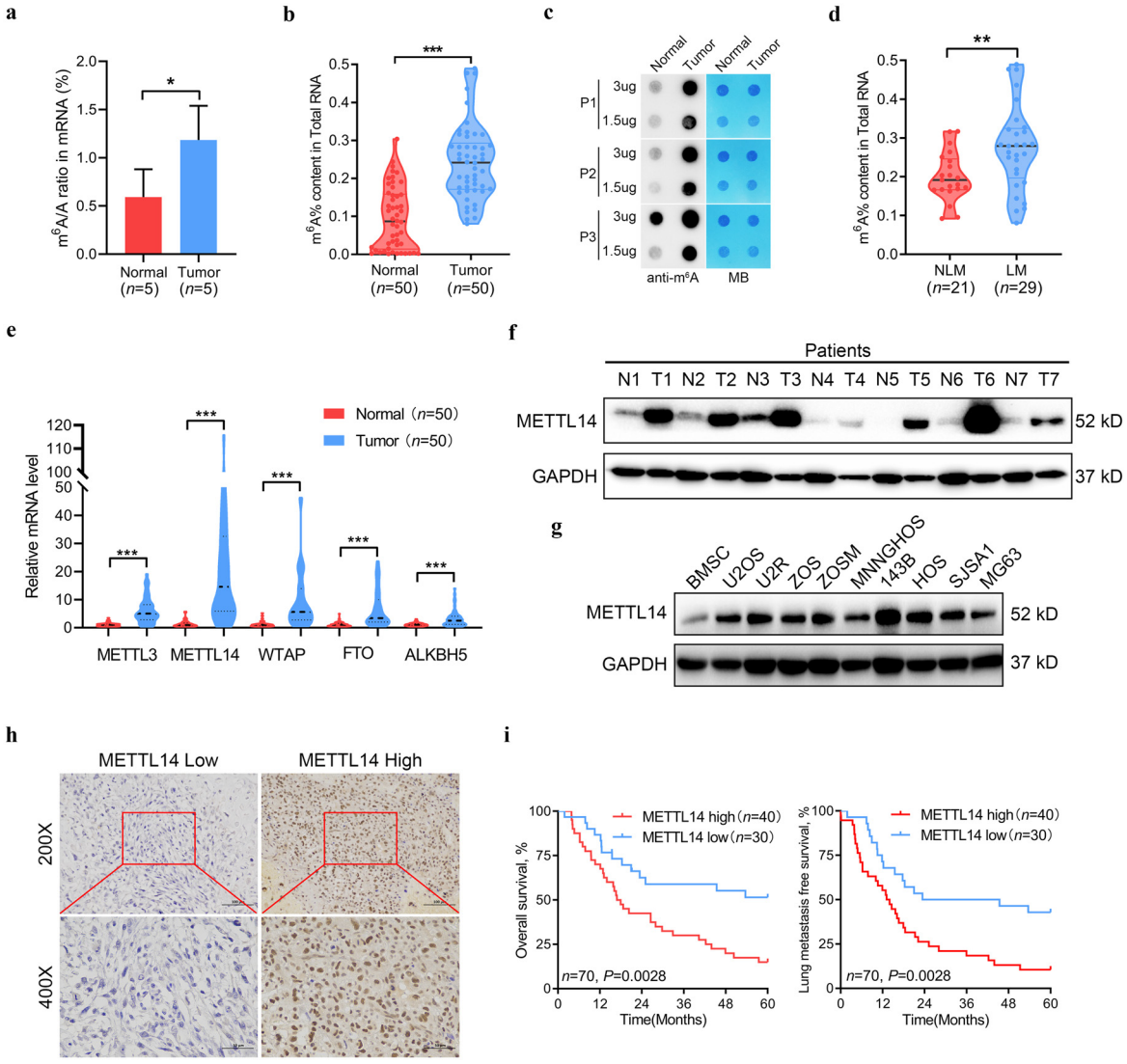

Figure 1. METTL14 is highly expressed in clinical osteosarcoma specimens and correlates with poor prognosis. (a) Global m^{6}A levels (m^{6}A/A) in mRNA in human OS tumor tissues versus tumor-adjacent tissues, as detected by liquid chromatography-tandem mass spectrometry (LC-MS/MS) (*n*=5). **(b)** The RNA *N*^{6}-methyladenosine (m^{6}A) levels in 50 paired OS tissues detected by colorimetric ELISA via an m^{6}A RNA methylation quantification kit (*n*=50). **(c)** The global mRNA m^{6}A level in human OS samples determined by RNA m^{6}A dot blot assay with an anti-m^{6}A antibody (left); methylene blue (MB) (right) staining served as the loading control (*n*=3). **(d)** The m^{6}A RNA levels in OS tumor tissues from patients with lung metastasis (LM, *n*=29) and without lung metastasis (NLM, *n*=21). **(e)** Expression of the m^{6}A regulatory enzymes in OS and paired normal tissues was measured by qPCR (*n*=50). **(f)** METTL14 protein levels in OS tissues and paired normal tissues, as detected by western blotting (*n*=7). **(g)** METTL14 protein levels in bone marrow stem cells (BMSCs) and nine OS cell lines, as detected by western blotting. **(h)** Representative immunohistochemistry (IHC) images showing METTL14 expression in OS patient tumor tissues (scale bars=100 μm or 50 μm, respectively). **(i)** Kaplan-Meier survival analysis of OS patients stratified by METTL14 expression level (*n*=70, p<0.05, log-rank test). * $p<0.05$; ** $p<0.01$; *** $p<0.001$, by independent Student's t test (**a, b**, and **d**) or log-rank test (**i**).

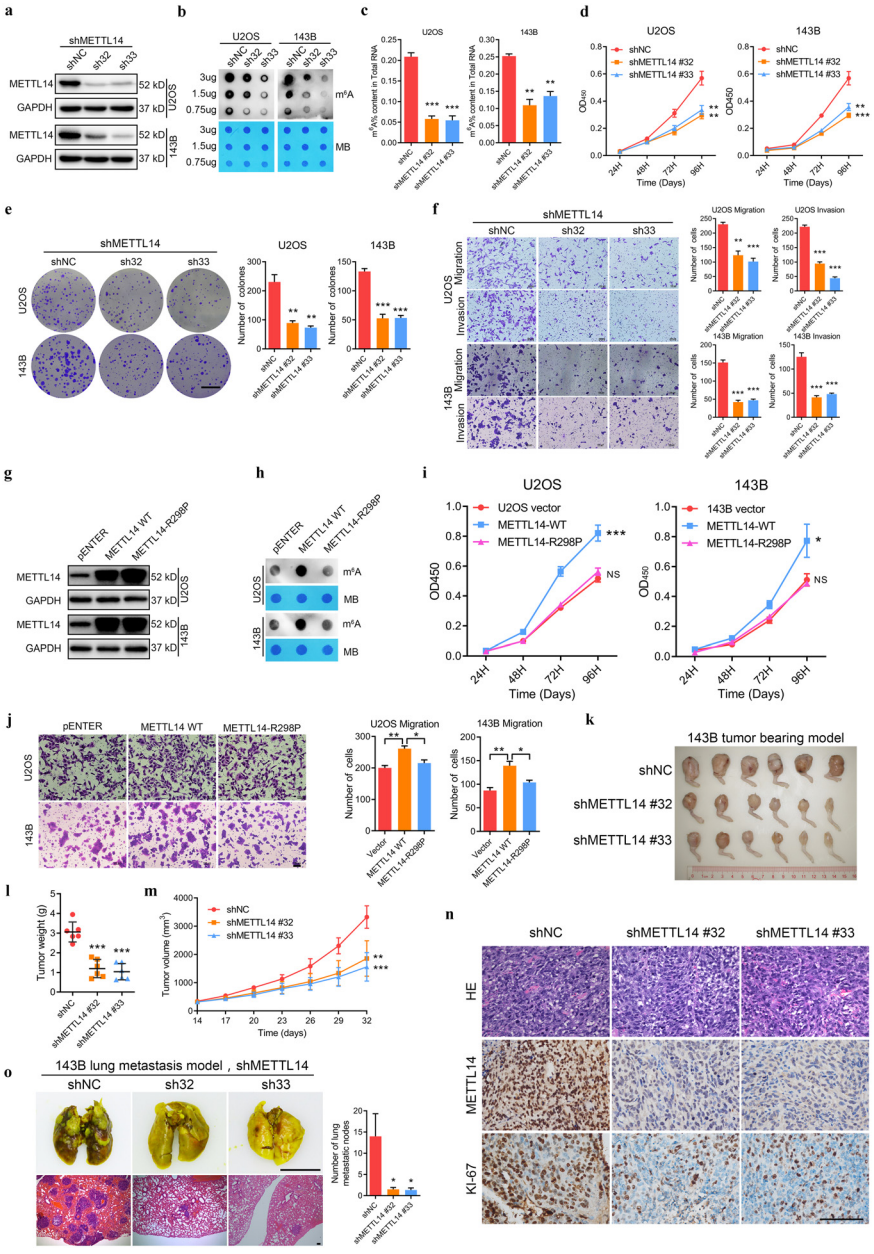

Figure 2. METTL14 promotes OS proliferation and metastasis *in vitro and in vivo*. **(a)** The protein levels of METTL14 in METTL14-KD U2OS and 143B cells, as measured by western blotting. **(b-c)** The global mRNA m^{6}A level in METTL14-KD U2OS and 143B cells, as determined by dot blot **(b)** with an m^{6}A antibody (upper panel), MB (bottom blue) staining served as a loading control and was detected by colorimetric ELISA **(c)** via an m^{6}A RNA methylation quantification kit. **(d-f)** The proliferation (**d**), colony formation (**e**), migration and invasion (**f**) abilities of METTL14-KD U2OS and 143B cells. Representative images and quantification of the colony formation (scale bars=1 cm), cell migration and invasion assay (scale bars=100 μm) results are shown. **(g-h)** The protein levels of METTL14 **(g)** according to western blotting and the global mRNA m^{6}A level **(h)** according to dot blot analyses with an m^{6}A antibody (upper panel), MB (bottom blue) staining served as a loading control in U2OS and 143B cells with wild-type (WT) METTL14 or catalytic mutant overexpression. **(i-j)** The proliferation (**i**) and migration (**j**) ability of U2OS and 143B cells overexpressing WT METTL14 or a catalytic mutant. Representative images and quantification of the cell migration assay results are shown (scale bars=100 μm). **(k)** Knockdown of METTL14 effectively inhibited 143B OS cell tumor growth in nude mice (*n*=6). **(l)** The tumors were extracted and weighed after 32 days. **(m)** The tumor volume was monitored every 3 days, and tumor growth curves were generated. **(n)** Sections of tumors were stained with hematoxylin and eosin (HE) and anti-METTL14 and anti-Ki-67 antibodies by IHC (scale bars=100 μm). **(o)** Knockdown of METTL14 significantly decreased 143B OS cell lung metastasis in nude mice. Left, representative lung (scale bars=1 cm) and HE staining of lung metastatic lesions (scale bars=100 μm); Right panel, the number of metastatic nodules formed in the lungs (*n*=6). The data are expressed as the mean±SD of three independent experiments. * $p<0.05$; ** $p<0.01$; *** $p<0.001$, by 1-way ANOVA.

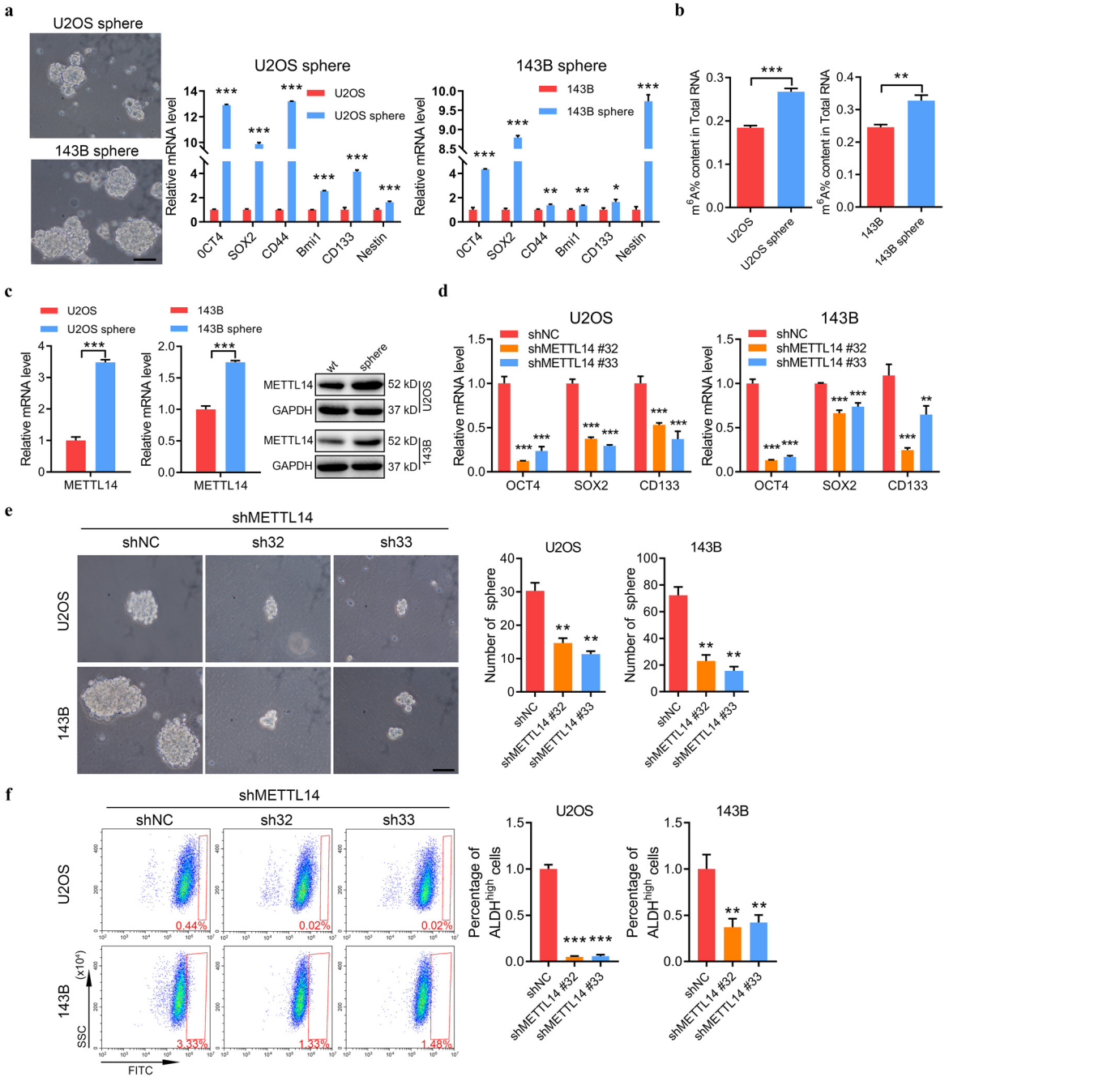

Figure 3. METTL14 maintains the stemness of OS cells. (a) Representative images of cancer stem cells (CSCs) isolated from U2OS and 143B cells (scale bars=100 μm) and the expression of stemness markers in CSCs, as determined by qPCR. **(b)** The global mRNA m^{6}A level in CSCs, as detected by colorimetric ELISA via the m^{6}A RNA methylation quantification kit. **(c)** The expression of METTL14 in CSCs, as measured by qPCR and western blotting. **(d)** The expression of stemness markers in METTL14-KD U2OS and 143B cells, as measured by qPCR. **(e)** Representative images and quantification of the in vitro sphere formation assay of METTL14-KD OS cells and control cells (n=3) (scale bars=100 μm). **(f)** ALDH activity in METTL14-KD U2OS and 143B cells, as determined by fluorescence-activated cell sorting analysis. Representative images and quantification of the ALDH activity results are shown. The data are expressed as the mean±SD of three independent experiments. * $p<0.05$; ** $p<0.01$; *** $p<0.001$, by independent Student's t test (**a, b**, and **c**) or 1-way ANOVA (**d, e**, and **f**).

MeRIP-seq and RNA-seq analyses identify MN1 as a downstream target of METTL14-mediated m^{6}A modification

To investigate the downstream target genes of METTL14 in OS, we then performed m^{6}A-modified RNA immunoprecipitation sequencing (MeRIP-seq) and RNA sequencing (RNA-seq) with stable METTL14-KD and control U2OS and 143B cells. MeRIP-seq revealed more than 1366 and 1816 differential m^{6}A peaks in U2OS and 143B cells (fold change >1.5, $p < 0.05$) (Figure 4(a)). The most common m^{6}A motif GGAC was significantly (p <5.3e-19) enriched in the m^{6}A peaks, and the m^{6}A peaks were especially enriched in the vicinity of the stop codon and 3′ untranslated region (3′ UTR), with 6.61% (U2OS) and 6.91% (143B) of peaks in the 5′ UTR (Figure 4(b) and (c)). As in previous studies, we considered the role of METTL14 in the m^{6}A writer complex and only considered m^{6}A peaks with decreased abundance (termed m^{6}A-hypo peaks) upon METTL14 knockdown to be authentic m^{6}A peaks. Based on this defined criteria, we discovered eight m^{6}A-hypo genes were associated with downregulated METTL14 mRNA levels in both METTL14-KD U2OS and 143B cells (Figure 4(d)). Among them, MN1 is the most downregulated gene which is chosen for further investigation (Figure 4(e)). Indeed, MeRIP-seq revealed that the m^{6}A modifications in the MN1 mRNA transcripts are markedly decreased in METTL14-KD OS cells (Figure 4(f)). Furthermore, immunoblotting and qRT-PCR assays showed that MN1 protein levels are downregulated in METTL14-KD OS cells (Figure 4(g) and (h)). Western blot also showed the increases in MN1 expression after METTL14 upregulation in OS cells (Figure S3). The m^{6}A level of MN1 exhibited the most consistent decrease in METTL14-KD OS cells compared to the control cells by m^{6}A-qPCR (Figure 4(i)). Together, our MeRIP-seq and RNA-seq studies suggest that MN1 is a novel downstream target of METTL14-mediated m^{6}A modification in OS.

METTL14 upregulates MN1 to promote OS malignancy in vitro and in vivo

To further characterize the oncogenic function of MN1 in OS, we first established stable MN1 knockdown (MN1-KD) models in U2OS and 143B cells (Figure 5(a)). Knockdown of MN1 dramatically suppressed the proliferation, colony formation, migration, and invasion abilities of U2OS and 143B cells (Figure 5(b-d)). A decrease in sphere number and size was also observed in MN1-KD U2OS and 143B cells compared with the control cells, and cancer stemness markers such as CD133, SOX2, and OCT4 were obviously reduced in MN1-KD U2OS and 143B cells (Figure 5(e-f), Figure S4(a)). We found that overexpression of MN1 rescues the proliferation, colony formation abilities of METTL14-KD cells (Figure 5(g-i)). To verify the relationship between MN1 and METTL14 *in vivo*, we performed tumor xenograft studies and observed that overexpression of MN1 in METTL14-KD 143B cells significantly increase the tumor growth rate, as reflected by the increases in xenograft tumor size and weight compared to those in the stable METTL14-KD cells (Figure 5(l) and (m)). These results together indicate that METTL14 upregulates MN1 to accelerate malignancy *in vitro* and *in vivo*.

METTL14 upregulates MN1 to induce ATRA resistance in OS

MN1 has been reported to induce resistance to ATRA in AML patients.[22,40] MN1 inhibits a large group of RAR/RXR-induced gene expression.[41] MN1-TEL can inhibit RAR-mediated transcription.[23] Numerous experiments and clinical trials have confirmed that ATRA and its derivatives are effective and promising drug used for treating APL and various other tumor types, including neuroblastoma, melanoma, and breast cancer.[25] However, there have been no advances in the clinical application of ATRA for OS treatment in the past two decades. Here, we found that the expression of MN1 and IC_{50} values for ATRA were much higher in U2OS and 143B cells than in AML patient-derived HL60 cells which can be killed with a combination of chemotherapy and ATRA (Figure 6(a) and Figure S5(a)). The sensitivity to ATRA was increased in MN1-KD and METTL14-KD U2OS and 143B cells compared to control cells, while ATRA resistance was restored after overexpression of MN1 in METTL14-KD cells (Figure 6(b) and Figure S5 (b)). Our tumor xenograft studies showed that tumor growth and weight are significantly decreased in the MN1-KD and METTL14-KD groups treated with ATRA compared to the DMSO group. The tumor growth and weight in the group with overexpression of MN1 in METTL14-KD cells treated with ATRA were not significantly decreased (Figure 6(c-e)). Immunostaining assays indicated that the growth-impaired tumors generated from METTL14-KD OS cells have lower expression of MN1 and Ki-67 than the control tumors (Figure 6(f)).Taken together, our ATRA resistance study indicates that METTL14 upregulates MN1 to induce ATRA resistance in OS.

METTL14 regulates the mRNA stability and translation of MN1 via IGF2BP2 in an m^{6}A-dependent manner

It has been confirmed that m^{6}A modification of mRNA transcripts regulates mRNA stability and translation.[12,14,42] To investigate whether METTL14-mediated m^{6}A modification affects the stability and translation of MN1 mRNA, we treated U2OS and 143B OS cells with the transcription inhibitor actinomycin D (Act D) and then detected the half-lives of MN1 transcripts. Indeed, the half-lives of MN1 transcripts were significantly decreased in METTL14-KD cells compared

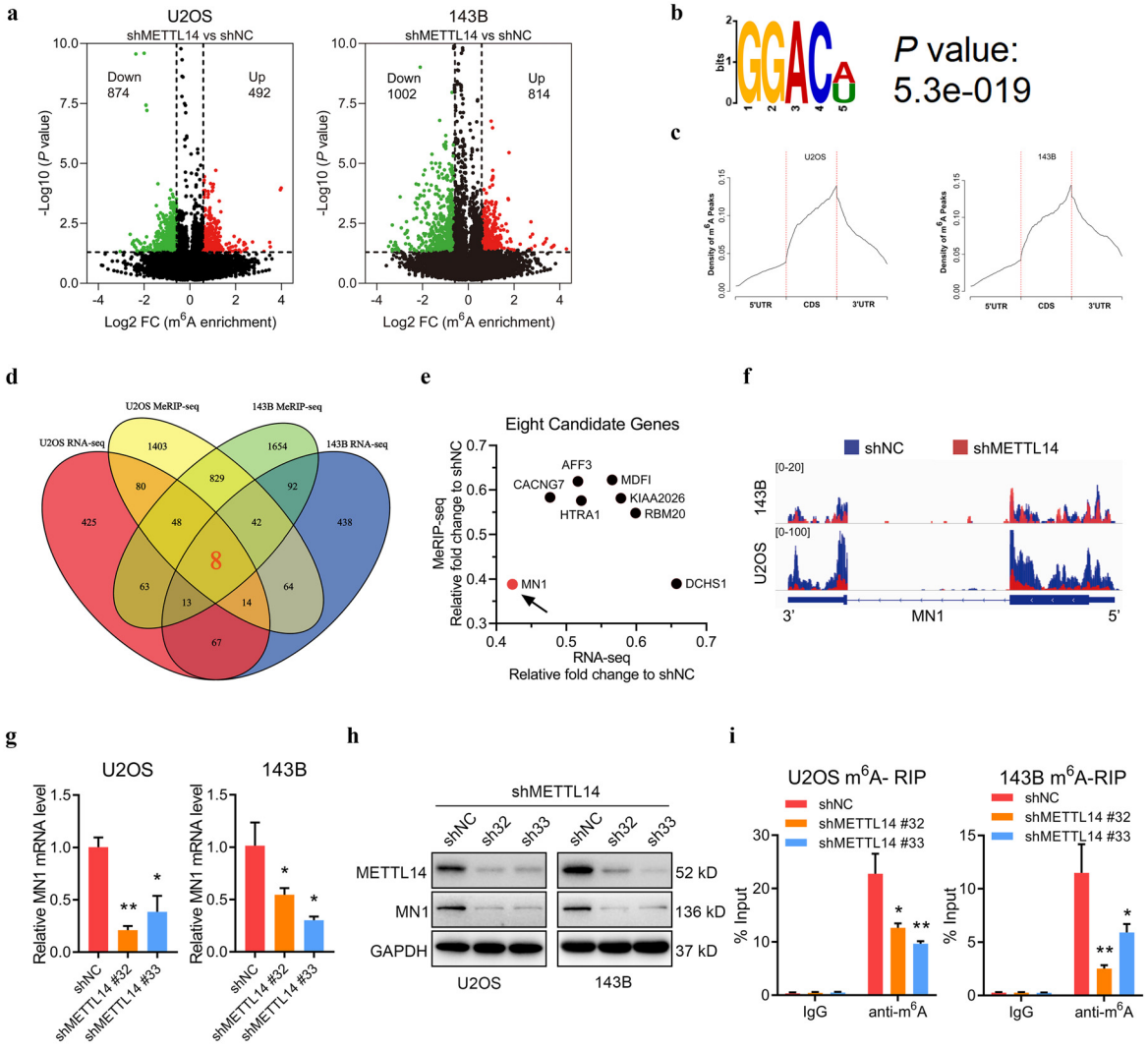

Figure 4. MeRIP-seq and RNA-seq analyses identify MN1 as a downstream target of METTL14-mediated m6A modification. **(a)** Volcano plots showing the numbers of significantly increased and decreased m^{6}A peaks (fold change > 1.5, $p < 0.05$) in METTL14-KD U2OS (left) and 143B (right) cells compared with control cells. **(b)** Top enriched motifs within m^{6}A peaks identified in U2OS and 143B cells. **(c)** Distribution of m^{6}A sites along the lengths of mRNA transcripts in U2OS and 143B cells. **(d)** RNA-seq and MeRIP-seq identified differentially expressed genes in stable METTL14-KD cells compared with their corresponding control cells. **(e)** Eight candidate genes in stable METTL14-KD cells. The X axis: RNA-seq analysis of the fold change in the expression of candidate mRNA transcripts; the Y axis: MeRIP-seq analysis of the enrichment of candidate mRNA transcripts. Both of these are the average values for stable METTL14-KD U2OS and 143B cells represented as fold change relative to shNC cells. **(f)** The m^{6}A abundance on MN1 mRNA transcripts in METTL14-KD and control U2OS and 143B cells, as detected by MeRIP-seq. **(g-h)** qPCR **(g)** and western blot **(h)** assays showing a decrease in MN1 expression after METTL14 knockdown in OS cell lines. **(i)** Reduction in the m^{6}A modification level of specific regions of MN1 transcripts upon METTL14 knockdown, as assessed by gene-specific m^{6}A-qPCR assay in U2OS (left) and 143B (right) cells. The data are expressed as the mean±SD of three independent experiments. * $p<0.05$; ** $p<0.01$; *** $p<0.001$, by 1-way ANOVA.

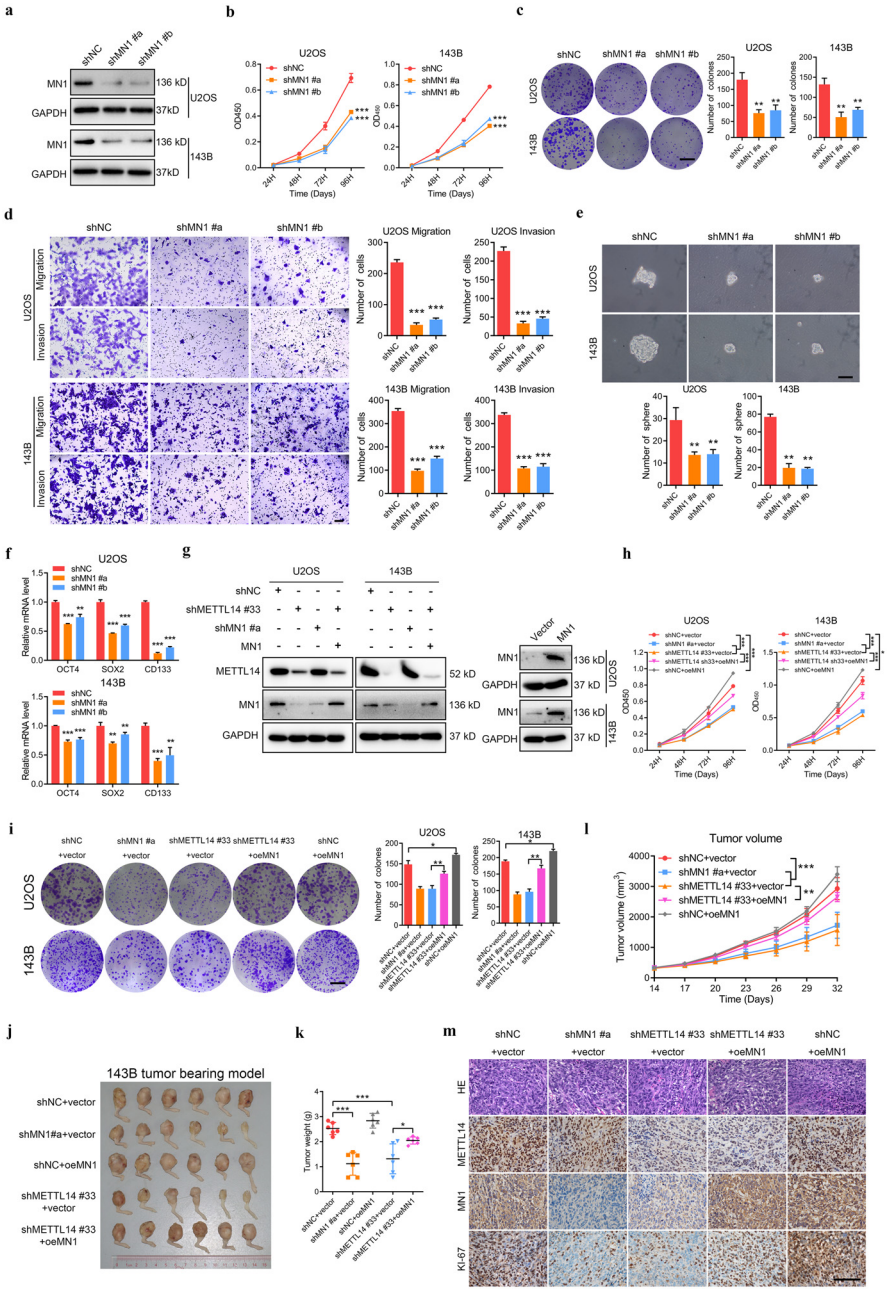

Figure 5. METTL14 upregulates MN1 to promote OS malignancy *in vitro and in vivo*. **(a)** The protein levels of MN1 in MN1-KD U2OS and 143B cells, as detected by western blotting. **(b-e)** Knockdown of MN1 significantly suppressed proliferation (**b**), colony formation (**c**), migration and invasion (**d**), and sphere formation (**e**) in U2OS and 143B cells. Representative images and quantification of the colony formation (scale bars=1 cm), cell migration and invasion (scale bars=100 μm), and sphere formation assay (scale bars=100 μm) results are shown. **(f)** The expression of stemness markers in MN1-KD U2OS and 143B cells, as measured by qPCR. **(g)** Western blots showing knockdown of METTL14 and MN1 as well as ectopic expression of MN1 in the corresponding groups compared to the empty vector groups. **(h-i)** MN1 overexpression rescues proliferation (**h**) and colony formation (**i**) in U2OS and 143B cells induced by METTL14 knockdown. Representative images and quantification of the colony formation assay results are shown (scale bars=1 cm). **(j)** Overexpression of MN1 rescues METTL14-induced 143B OS cell orthotopic tumor growth in nude mice (n=6). **(k)** The tumors were extracted and weighed after 32 days. **(l)** The tumor volume was monitored every 3 days, and tumor growth curves were generated. **(m)** Sections of tumors were stained with HE and with anti-MN1, anti-METTL14 and anti-Ki-67 antibodies by IHC (scale bars=100 μm). The data are expressed as the mean±SD of three independent experiments. * $p<0.05$; ** $p<0.01$; *** $p<0.001$, by 1-way ANOVA.

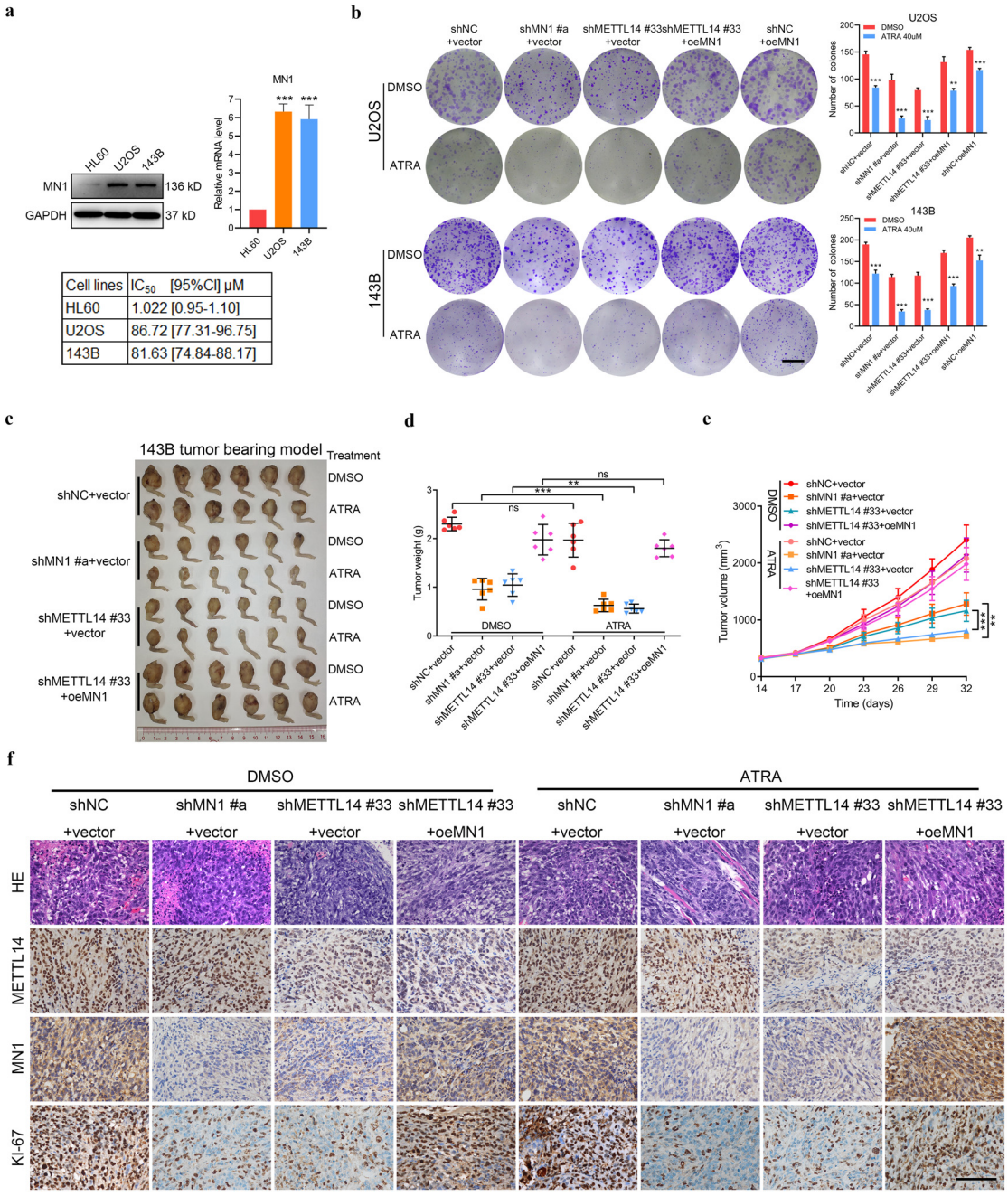

Figure 6. METTL14 upregulates MN1 to induce ATRA resistance in OS (a) The MN1 expression as detected by Western blot and qPCR assays, and the IC_{50} values of ATRA as detected by CCK8 in U2OS, 143B and HL60 cells. **(b)** All-trans-retinoic acid (ATRA) impaired the colony formation of METTL14-KD, MN1-KD and control U2OS and 143B cells with or without MN1 overexpression. The colony formation ability was examined after treatment with 40 μM of ATRA for 10 days. The quantification of cell growth in the right panel is presented as the mean ± SD (scale bars=1 cm). **(c)** ATRA suppressed OS growth in an orthotopic mouse model. Tumor growth curves of mice treated with either vehicle or ATRA for 14 days (25 mg/kg once every three days by intraperitoneal [i.p.] injection) (*n*=6). **(d)** The tumors were extracted and weighed after 32 days. Data represent mean ± SD. **(e)** The tumor volume was monitored every 3 days, and tumor growth curves were generated. **(f)** Sections of tumors were stained with HE and with anti-MN1, anti-METTL14 and anti-Ki-67 antibodies by IHC (scale bars=100 μm). The data are expressed as the mean±SD of three independent experiments. * $p<0.05$; ** $p<0.01$; *** $p<0.001$, by independent Student's t test.

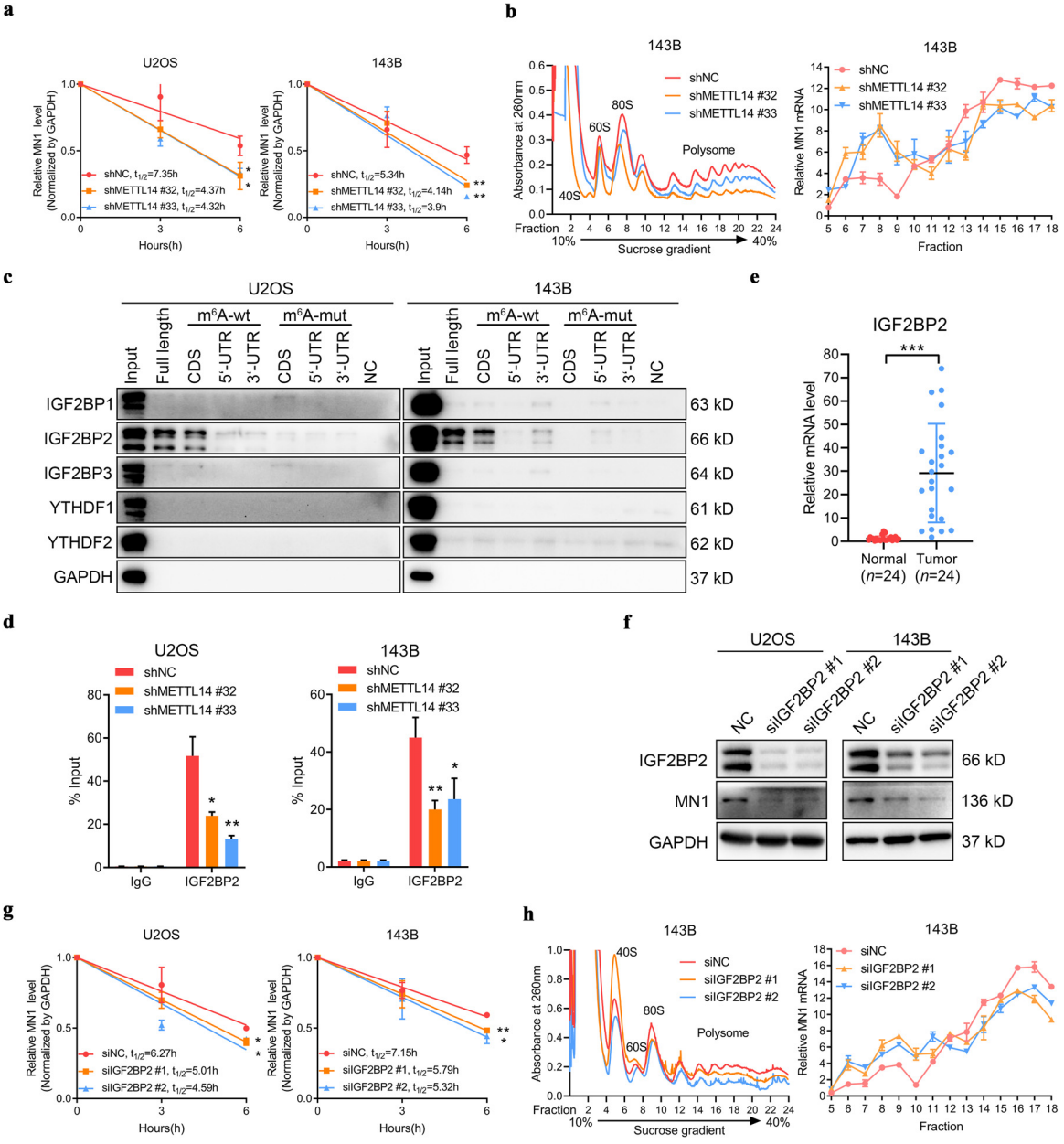

Figure 7. METTL14 regulates the mRNA stability and translation of MN1 via IGF2BP2 in an m^{6}A-dependent manner. (a) The mRNA decay rate analysis and the qPCR analysis of MN1 at the indicated times after actinomycin D (Act D, 5 μg/ml) treatment in U2OS and 143B cells after METTL14 inhibition. **(b)** Polysome profiling assays. The fractionation of lysates from 143B cells with or without METTL14 knockdown is shown on the left. RNAs in different ribosome fractions were extracted and subjected to qPCR analysis. **(c)** Western blotting of IGF2BP1/2/3 and YTHDF1/2 after RNA pull-down assay with the cell lysate (Ly.), full-length biotinylated MN1, MN1 CDS, 3′UTR and 5′UTR with or without the m^{6}A motif mutation, and beads only (NC) in U2OS and 143B cells. **(d)** RIP-qPCR showing the enrichment of MN1 in U2OS and 143B cells after METTL14 inhibition. **(e)** The expression of IGF2BP2 in OS and paired normal tissues was measured by qPCR (n=24). **(f)** Western blotting of MN1 after IGF2BP2 inhibition in U2OS and 143B cells. **(g)** The mRNA decay rate analysis and qPCR analysis of MN1 at the indicated times after Act D (5 μg/ml) treatment in U2OS and 143B cells after IGF2BP2 inhibition. **(h)** Polysome profiling assays. The fractionation of lysates from 143B cells with or without IGF2BP2 knockdown is shown on the left. RNAs in different ribosome fractions were extracted and subjected to qPCR analysis. The data are expressed as the mean±SD of three independent experiments. * $p<0.05$; ** $p<0.01$; *** $p<0.001$, by independent Student's t test (**e**) or 1-way ANOVA (**a, b, d, g** and **h**).

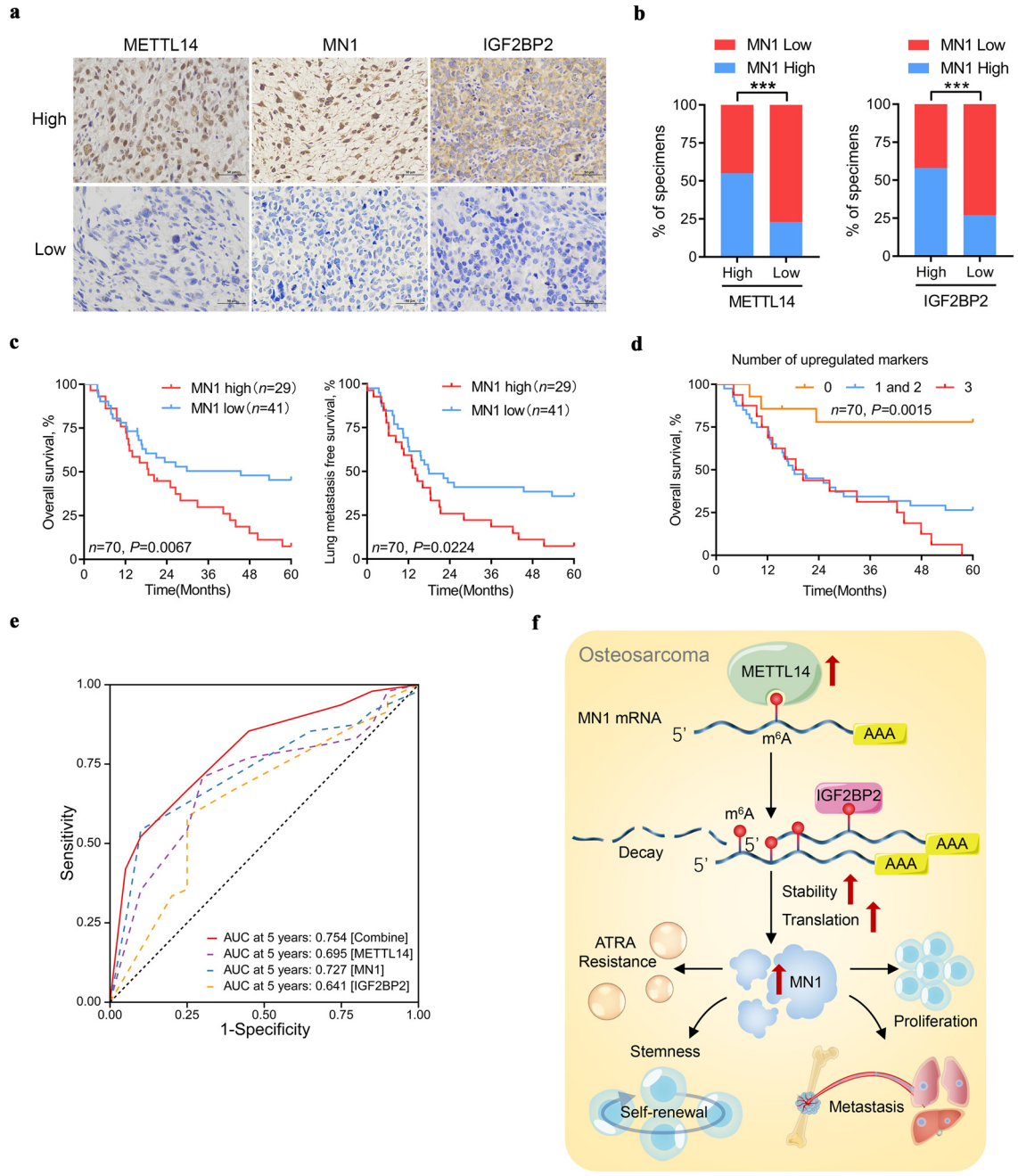

Figure 8. Clinical correlation between METTL14, MN1, and IGF2BP2 in OS. (a) Representative images showing high or low expression of METTL14, MN1 and IGF2BP2 in OS tumor specimens (scale bars=100 μm). **(b)** Correlation between MN1 and METTL14 or IGF2BP2 in OS microarray specimens. **(c)** Kaplan–Meier survival analysis of MN1 expression in patients with OS (n=70, p<0.05, log-rank test). **(d)** Kaplan–Meier analysis of overall survival for OS patients (n =70) based on the number of upregulated molecular markers (Kaplan–Meier analysis with log-rank test). Patients were stratified into groups based on the individual median expression levels of METTL14, MN1, and IGF2BP2 expression according to IHC analysis, and the patients were divided into three groups as indicated. **(e)** Receiver operating characteristic (ROC) curve analysis for 5-year survival for METTL14 [AUC = 0.695, (95% CI, 0.563–0.827)], MN1 [AUC = 0.727, (95% CI, 0.610–0.845)], and IGF2BP2 [AUC = 0.641, (95% CI, 0.497–0.784)] as individual biomarkers or for the combined panel [AUC = 0.754 (95% CI, 0.635–0.873)]. AUC, area under the curve. **(f)** Graphic illustration of METTL14 contributing to OS progression and ATRA resistance through m^6A-IGF2BP2-dependent posttranscriptional modification of MN1. * p<0.05; ** p<0.01; *** p<0.001, by Pearson's *chi*-squared test (**b**) or log-rank test (**c**, and **d**).

with control cells (Figure 7(a)). Furthermore, we performed polysome profiling analysis and found that knockdown of METTL14 resulted in a decrease in MN1 mRNA in the translation pool, suggesting METTL14-mediated m^{6}A modification affects both stability and translation of MN1 mRNA in 143B cells (Figure 7(b), Figure S6(a)). It has been shown that the effect of m^{6}A modification on mRNA transcripts is mediated by m^{6}A readers which are specific m^{6}A binding proteins. Recent studies have pointed out IGF2BPs and YTH family proteins are two major families of m^{6}A readers and play an essential role in regulating the fate of methylated mRNA.[12–14] To explore the specific m^{6}A binding proteins regulating m^{6}A-methylated MN1 mRNA, we performed an RNA pull-down assay with several classical m^{6}A readers. Our results showed that IGF2BP2 obviously binds to the full-length MN1 transcripts in U2OS and 143B cells. IGF2BP2 mostly bound to the CDS region instead of the 5' UTR or 3' UTR of MN1 transcripts, and the specific binding to the MN1 transcript was significantly impaired when m^{6}A motifs were deleted (Figure 7(c)). On the other hand, compared to the IgG control the IGF2BP2-specific antibody significantly enriched MN1 mRNA in the RIP-qPCR assays in U2OS and 143B cells, and the enrichment of MN1 mRNA by the IGF2BP2 pull down was significantly impaired after knockdown of METTL14 (Figure 7(d)). The elevated expression of IGF2BP2 was observed in OS samples (Figure 7(e)). Knockdown of IGF2BP2 suppressed MN1 mRNA and protein expression (Figure 7(f)). Overexpression of IGF2BP2 promoted the protein expression of MN1 in OS cells (Figure S6(b)). The half-lives of MN1 transcripts and the MN1 translational efficiency were significantly decreased in IGF2BP2 knockdown (IGF2BP2-KD) cells compared with control cells (Figure 7(g-h), Figure S6(c)). Taken together, our findings indicate that METTL14-mediated m^{6}A modification maintains MN1 expression in an m^{6}A-IGF2BP2-dependent manner by regulating MN1 mRNA stability and translation.

Clinical correlation between METTL14, MN1, and IGF2BP2 in OS

To further investigate whether the aforementioned conclusions could be supported in human primary OS, we study the expression of METTL14, MN1, and IGF2BP2 in 70 human primary OS specimens by IHC staining (Figure 8(a)). The expression of MN1 was positively correlated with the expression of both METTL14 and IGF2BP2 in OS tissues (Figure 8(b)). Furthermore, Kaplan-Meier analysis suggested that high expression of MN1 notably correlates with poor prognosis in OS patients (Figure 8(c)). High IGF2BP2 expression had a relative poorer prognosis in OS patients, although it was not statistically significant (p=0.0566, log-rank test) (Figure S7). OS patients with high levels of METTL14, MN1, and IGF2BP2 had the shortest overall survival times (Figure 8(d)). Moreover, receiver operating characteristic (ROC) curve analysis indicated that the combination index of the IHC panel (METTL14, MN1, and IGF2BP2) present additive predictive value for overall survival (Figure 8(e)), indicating its superiority over any individual marker for evaluating the prognosis of OS patients. The tumor immunohistochemical staining data further strengthened the notion that METTL14/IGF2BP2 axis in regulating MN1 mRNA stability and translation by m^{6}A epitranscriptome regulatory machinery and is associated with poor clinical outcome of OS patients. In summary, on the basis of our findings, we propose a model in whichMETTL14/MN1 axis promotes OS progression partly by regulating the stability and translation efficiency of MN1 and induces ATRA resistance (Figure 8(f)).

Discussion

The m^{6}A is the most abundant mRNA modification among numerous RNA modifications.[7,42] Recent reports have shown that m^{6}A modification exerts essential but varying biological functions in the progression of various cancers,[43] such as leukemia,[44] endometrial cancer,[17] liver cancer,[18,19] and glioma,[45] regulating the expression of specific oncogenes or tumor suppressor genes at the epigenetic transcription level. The m^{6}A modification regulates RNA biological functions via m^{6}A methyltransferases, demethylases, and readers.[46–49] METTL14, a key component of the m^{6}A methyltransferase complex, can stabilize the structure of METTL3, enhance the enzyme activity of METTL3 by binding with RNA, and affect the overall m^{6}A level.[50] The METTL3-METTL14 complex displayed much higher catalytic activity than either METTL3 or METTL14 alone.[50] METTL14 plays an essential regulatory role in the occurrence and development of malignant tumors.[51] Previous studies have reported that METTL14 promotes MYC mRNA stability and translation and plays an essential oncogenic role in leukemia.[16] METTL14 can regulate AKT activity to promote the proliferation and tumorigenicity of endometrial cancer through an m^{6}A-dependent regulatory mechanism.[17] It has also been reported that METTL14 suppresses the metastatic potential of hepatocellular carcinoma by processing primary miRNAs in an m^{6}A-dependent manner.[18] Several studies have reported that METTL3 promotes malignant phenotypes of osteosarcoma cells via RNA m^{6}A modification mechanisms.[52–56] However, the studies of METTL14 in osteosarcoma were still limited, and the function of METTL14 remained vague. Huan et al. reported that METTl3/METTL14 regulated DIRAS1/p-ERK signaling to promote malignant behaviors of osteosarcoma cells.[53] Li et al. found low expression of METTL14 was significantly associated with poor prognosis of osteosarcoma patients.[57] Liu et al. reported

that METTL14 overexpression promoted osteosarcoma cell apoptosis and inhibited tumor progression.[58] In our study, we found that the m^{6}A RNA modification levels are significantly elevated in OS tissues, especially in OS tissues with lung metastasis. We demonstrated that METTL14 induces an increase in m^{6}A modification in OS, facilitates OS proliferation and metastasis *in vitro* and *in vivo*, and promotes OS cell stemness. METTL14 regulated the expression of a series of mRNA transcripts, and this function was dependent on its m^{6}A catalytic activity. The high expression of METTL14 was associated with a poor prognosis in OS patients, which suggests that METTL14 could be a biomarker for OS prognosis and treatment.

To elucidate the molecular mechanisms involved in METTL14-mediated osteosaarcomagenesis, we adapted systems approaches using MeRIP-seq and RNA-seq to identify MN1 as a downstream target gene of METTL14. The interaction between METTL14 and MN1 is dependent on the m^{6}A catalytic activity of METTL14. The oncoprotein MN1 has been reported to be a TEL fusion protein and an overexpressed gene in AML.[21,40] High expression of MN1 indicates a poor prognosis in AML patients.[24] MN1 acts as a highly effective hematopoietic oncogene, and its overexpression induces AML in mice.[22] MN1 is one of the stemness genes critical for leukemogenicity, and overexpression of MN1 promotes proliferation/self-renewal and blocks differentiation.[22,59] Our results suggest that MN1 acts as an oncogene to promote OS proliferation and metastasis *in vitro* and *in vivo* as well as OS cell stemness.

The biological functions of m^{6}A modification depend on m^{6}A binding proteins, which are called m^{6}A readers, including IGF2BP1/2/3 and the YTH family, which regulate RNA metabolism, including translation, splicing, export, and degradation.[12–14] For instance, YTHDF1 mediates the nuclear export and translation of mRNA,[15] and YTHDF2 regulates mRNA stability and RNA structural remodeling.[14] The m^{6}A reader protein IGF2BP2 has been identified to preferentially recognize m^{6}A-modified mRNAs and promote their stability and translation.[13] Our findings determined that IGF2BP2 specifically binds to the CDS regions of MN1 transcripts and regulates the mRNA half-life of MN1 in an m^{6}A-dependent manner. We also found that IGF2BP2 facilitates MN1 mRNA translation through an m^{6}A-dependent regulatory mechanism. The expression levels of IGF2BP2 were also elevated in OS samples. These results indicate METTL14 mediates m^{6}A demethylation on MN1 mRNA to promote its stability and translation via an IGF2BP2-dependent mechanism.

ATRA, an active metabolite of vitamin A, has been confirmed to be an effective and promising drug for treating various cancers.[60] ATRA has been used in the treatment of acute promyelocytic leukemia (APL) for decades and has revolutionized the outcomes of patients with APL. More than 80–90% of APL patients are expected to be cured with a combination of ATRA, arsenic trioxide and/or chemotherapy.[61] Treatment with ATRA can induce morphologic changes and osteogenic differentiation in osteosarcoma cell lines.[26–28] ATRA, combined with 22-oxa-calcitriol, could inhibit the growth and pulmonary metastasis of osteosarcoma *in vivo*.[29] Todesco et al. showed that combined treatment with ATRA/IFNa yielded partial remission for a boy aged 14 years with stage IIB small cell OS.[30] ATRA based regiment was considered as an alternative approach in the treatment of patients with osteosarcoma. However, there have been no advances in the clinical application of ATRA for OS treatment in the past two decades. Here, we identified that the inhibition of OS by ATRA was negatively correlated with the expression of METTL14 and MN1, which is regulated by METTL14 through m^{6}A methylation. MN1 has been reported to inhibit a large group of RAR/RXR-induced gene expression and induce resistance to the differentiation-inducing agent ATRA both in cells and in AML patients.[41] MN1-TEL can inhibit RAR-mediated transcription.[23] Overexpression of MN1 induces AML in mice and predicts ATRA resistance in patients with AML.[22] Currently, the MAP regimen (high-dose methotrexate, cisplatin, and doxorubicin) is the primary first-line treatment in osteosarcoma. However, the effective drugs are limited once the first-line treatment fails, according to NCCN Guideline.[62] Our results suggest that ATRA treatment could probably be considered a promising complementary therapy in OS patients, especially in OS patients with low expression of METTL14 and/or MN1. Taken together, our results provide an important molecular foundation for ATRA treatment, suggest novel drug targets and will improve the treatment of OS. In addition, our findings about METTL14-IGF2BP2-MN1 panel provide an underlying biomarker panel for prognosis prediction in OS patients.

In conclusion, we revealed the critical role of METTL14 in OS progression and ATRA resistance and showed that this role is dependent on its m^{6}A catalytic activity. Mechanistically, METTL14 mediates m^{6}A demethylation of MN1 mRNA to promote its stability and translation via an IGF2BP2-dependent mechanism in OS. Our work suggests that METTL14 might be a potential prognostic predictor and therapeutic target for OS patients and provides an essential molecular foundation for ATRA treatment against OS.

Contributors

Conception and design: X. Xie, J. Shen

Development of methodology: H. Li, G. Huang, J. Tu, X. Xie, J. Shen

Acquisition of data (provided animals, acquired and managed patients, provided facilities, etc.): H. Li, G. Huang, J. Tu, D. Lv

Analysis and interpretation of data (e.g., statistical analysis, biostatistics, computational analysis): H. Li, G. Huang, J. Tu, D. Lv, Q. Jin, J. Chen, Y. Zou

Writing, review, and/or revision of the manuscript: H. Li, J. Tu, G. Huang, D. Lee, X. Xie, J. Shen
Administrative, technical, or material support (i.e., reporting or organizing data, constructing databases): G. Huang, D. Lee, X. Xie, J. Shen
Study supervision: X. Xie, J. Shen
J. Tu, D. Lv, and Q. Jin have verified the underlying data. All the authors read and approved the final manuscript.

Data sharing statement

RNA-seq and MeRIP-seq data generated in this study have been deposited in GEO (GSE173519 and GSE173520).

Declaration of interests

No potential conflicts of interest were disclosed.

Acknowledgments

The authors thank all members of the Xie's laboratory for their advice and technical assistance. This work was supported by the National Natural Science Foundation of China (Grants 81972510 and 81772864).

Supplementary materials

Supplementary material associated with this article can be found in the online version at doi:10.1016/j.ebiom.2022.104142.

References

1 Biermann JS, Adkins D, Benjamin R, et al. Bone cancer. *J Natl Compr Canc Netw*. 2007;5(4):420–437.
2 Mirabello L, Troisi RJ, Savage SA. Osteosarcoma incidence and survival rates from 1973 to 2004: data from the surveillance, epidemiology, and end results program. *Cancer*. 2009;115(7):1531–1543.
3 Valery PC, Laversanne M, Bray F. Bone cancer incidence by morphological subtype: a global assessment. *Cancer Causes Control*. 2015;26(8):1127–1139.
4 Kansara M, Teng MW, Smyth MJ, Thomas DM. Translational biology of osteosarcoma. *Nat Rev Cancer*. 2014;14(11):722–735.
5 Bernthal NM, Federman N, Eilber FR, et al. Long-term results (>25 years) of a randomized, prospective clinical trial evaluating chemotherapy in patients with high-grade, operable osteosarcoma. *Cancer*. 2012;118(23):5888–5893.
6 Laschi M, Bernardini G, Geminiani M, et al. Establishment of four new human primary cell cultures from chemo-naive italian osteosarcoma patients. *J Cell Physiol*. 2015;230(11):2718–2727.
7 Lan Q, Liu PY, Haase J, Bell JL, Huttelmaier S, Liu T. The critical role of RNA m(6)A methylation in cancer. *Cancer Res*. 2019;79(7):1285–1292.
8 Meyer KD, Jaffrey SR. The dynamic epitranscriptome: N6-methyladenosine and gene expression control. *Nat Rev Mol Cell Biol*. 2014;15(5):313–326.
9 Vu LP, Cheng Y, Kharas MG. The biology of m(6)A RNA methylation in normal and malignant hematopoiesis. *Cancer Discov*. 2019;9(1):25–33.
10 Jiang Q, Crews LA, Holm F, Jamieson CHM. RNA editing-dependent epitranscriptome diversity in cancer stem cells. *Nat Rev Cancer*. 2017;17(6):381–392.
11 Tong J, Flavell RA, Li HB. RNA m(6)A modification and its function in diseases. *Front Med*. 2018;12(4):481–489.
12 Wang X, Zhao BS, Roundtree IA, et al. N(6)-methyladenosine modulates messenger RNA translation efficiency. *Cell*. 2015;161(6):1388–1399.
13 Huang H, Weng H, Sun W, et al. Recognition of RNA N(6)-methyladenosine by IGF2BP proteins enhances mRNA stability and translation. *Nat Cell Biol*. 2018;20(3):285–295.
14 Wang X, Lu Z, Gomez A, et al. N6-methyladenosine-dependent regulation of messenger RNA stability. *Nature*. 2014;505(7481):117–120.
15 Roundtree IA, Luo GZ, Zhang Z, et al. YTHDC1 mediates nuclear export of N(6)-methyladenosine methylated mRNAs. *Elife*. 2017;6:e31311.
16 Weng H, Huang H, Wu H, et al. METTL14 inhibits hematopoietic stem/progenitor differentiation and promotes leukemogenesis via mRNA m(6)A modification. *Cell Stem Cell*. 2018;22(2):191–205.e9.
17 Liu J, Eckert MA, Harada BT, et al. m(6)A mRNA methylation regulates AKT activity to promote the proliferation and tumorigenicity of endometrial cancer. *Nat Cell Biol*. 2018;20(9):1074–1083.
18 Ma JZ, Yang F, Zhou CC, et al. METTL14 suppresses the metastatic potential of hepatocellular carcinoma by modulating N(6) -methyladenosine-dependent primary MicroRNA processing. *Hepatology*. 2017;65(2):529–543.
19 Chen M, Wei L, Law CT, et al. RNA N6-methyladenosine methyltransferase-like 3 promotes liver cancer progression through YTHDF2-dependent posttranscriptional silencing of SOCS2. *Hepatology*. 2018;67(6):2254–2270.
20 Wang Q, Chen C, Ding Q, et al. METTL3-mediated m(6)A modification of HDGF mRNA promotes gastric cancer progression and has prognostic significance. *Gut*. 2020;69(7):1193–1205.
21 Buijs A, Sherr S, van Baal S, et al. Translocation (12;22) (p13;q11) in myeloproliferative disorders results in fusion of the ETS-like TEL gene on 12p13 to the MN1 gene on 22q11. *Oncogene*. 1995;10(8):1511–1519.
22 Heuser M, Argiropoulos B, Kuchenbauer F, et al. MN1 overexpression induces acute myeloid leukemia in mice and predicts ATRA resistance in patients with AML. *Blood*. 2007;110(5):1639–1647.
23 van Wely KH, Meester-Smoor MA, Janssen MJ, Aarnoudse AJ, Grosveld GC, Zwarthoff EC. The MN1-TEL myeloid leukemia-associated fusion protein has a dominant-negative effect on RAR-RXR-mediated transcription. *Oncogene*. 2007;26(39):5733–5740.
24 Heuser M, Beutel G, Krauter J, et al. High meningioma 1 (MN1) expression as a predictor for poor outcome in acute myeloid leukemia with normal cytogenetics. *Blood*. 2006;108(12):3898–3905.
25 Zhang L, Zhou Q, Zhang N, et al. E2F1 impairs all-trans retinoic acid-induced osteogenic differentiation of osteosarcoma via promoting ubiquitination-mediated degradation of RARalpha. *Cell Cycle*. 2014;13(8):1277–1287.
26 Yang QJ, Zhou LY, Mu YQ, et al. All-trans retinoic acid inhibits tumor growth of human osteosarcoma by activating Smad signaling-induced osteogenic differentiation. *Int J Oncol*. 2012;41(1):153–160.
27 Ying M, Zhang L, Zhou Q, et al. The E3 ubiquitin protein ligase MDM2 dictates all-trans retinoic acid-induced osteoblastic differentiation of osteosarcoma cells by modulating the degradation of RARalpha. *Oncogene*. 2016;35(33):4358–4367.
28 Luo P, Yang X, Ying M, et al. Retinoid-suppressed phosphorylation of RARalpha mediates the differentiation pathway of osteosarcoma cells. *Oncogene*. 2010;29(19):2772–2783.
29 Barroga EF, Kadosawa T, Okumura M, Fujinaga T. Inhibitory effects of 22-oxa-calcitriol and all- trans retinoic acid on the growth of a canine osteosarcoma derived cell-line in vivo and its pulmonary metastasis in vivo. *Res Vet Sci*. 2000;68(1):79–87.
30 Todesco A, Carli M, Iacona I, Frascella E, Ninfo V, Rosolen A. All-trans retinoic acid and interferon-alpha in the treatment of a patient with resistant metastatic osteosarcoma. *Cancer*. 2000;89(12):2661–2666.
31 Zou CY, Wang J, Shen JN, et al. Establishment and characteristics of two syngeneic human osteosarcoma cell lines from primary tumor and skip metastases. *Acta Pharmacol Sin*. 2008;29(3):325–332.
32 Dominissini D, Moshitch-Moshkovitz S, Salmon-Divon M, Amariglio N, Rechavi G. Transcriptome-wide mapping of N(6)-methyladenosine by m(6)A-seq based on immunocapturing and massively parallel sequencing. *Nat Protoc*. 2013;8(1):176–189.
33 Chen CY, Ezzeddine N, Shyu AB. Messenger RNA half-life measurements in mammalian cells. *Methods Enzymol*. 2008;448:335–357.
34 Gandin V, Sikstrom K, Alain T, et al. Polysome fractionation and analysis of mammalian translatomes on a genome-wide scale. *J Vis Exp*. 2014(87):51455.

35 Berlin O, Samid D, Donthineni-Rao R, Akeson W, Amiel D, Woods Jr. VL. Development of a novel spontaneous metastasis model of human osteosarcoma transplanted orthotopically into bone of athymic mice. *Cancer Res*. 1993;53(20):4890–4895.
36 Wang Y, Li Y, Toth JI, Petroski MD, Zhang Z, Zhao JC. N6-methyladenosine modification destabilizes developmental regulators in embryonic stem cells. *Nat Cell Biol*. 2014;16(2):191–198.
37 Peng F, Xu J, Cui B, et al. Oncogenic AURKA-enhanced N(6)-methyladenosine modification increases DROSHA mRNA stability to transactivate STC1 in breast cancer stem-like cells. *Cell Res*. 2020.
38 Huang H, Wang Y, Kandpal M, et al. FTO-dependent N (6)-methyladenosine modifications inhibit ovarian cancer stem cell self-renewal by blocking cAMP signaling. *Cancer Res*. 2020;80 (16):3200–3214.
39 Zhang Y, Kang M, Zhang B, et al. m(6)A modification-mediated CBX8 induction regulates stemness and chemosensitivity of colon cancer via upregulation of LGR5. *Mol Cancer*. 2019;18(1):185.
40 Carella C, Bonten J, Sirma S, et al. MN1 overexpression is an important step in the development of inv(16) AML. *Leukemia*. 2007;21(8):1679–1690.
41 Meester-Smoor MA, Janssen MJ, Grosveld GC, et al. MN1 affects expression of genes involved in hematopoiesis and can enhance as well as inhibit RAR/RXR-induced gene expression. *Carcinogenesis*. 2008;29(10):2025–2034.
42 Zhao BS, Roundtree IA, He C. Post-transcriptional gene regulation by mRNA modifications. *Nat Rev Mol Cell Biol*. 2017;18(1):31–42.
43 Chen B, Li Y, Song R, Xue C, Xu F. Functions of RNA N6-methyladenosine modification in cancer progression. *Mol Biol Rep*. 2019;46(2):2567–2575.
44 Vu LP, Pickering BF, Cheng Y, et al. The N(6)-methyladenosine (m (6)A)-forming enzyme METTL3 controls myeloid differentiation of normal hematopoietic and leukemia cells. *Nat Med*. 2017;23 (11):1369–1376.
45 Visvanathan A, Patil V, Arora A, et al. Essential role of METTL3-mediated m(6)A modification in glioma stem-like cells maintenance and radioresistance. *Oncogene*. 2018;37(4):522–533.
46 Lin S, Choe J, Du P, Triboulet R, Gregory RI. The m(6)A methyltransferase METTL3 promotes translation in human cancer cells. *Mol Cell*. 2016;62(3):335–345.
47 Barbieri I, Tzelepis K, Pandolfini L, et al. Promoter-bound METTL3 maintains myeloid leukaemia by m(6)A-dependent translation control. *Nature*. 2017;552(7683):126–131.
48 Li Z, Weng H, Su R, et al. FTO plays an oncogenic role in acute myeloid leukemia as a N(6)-methyladenosine RNA demethylase. *Cancer Cell*. 2017;31(1):127–141.
49 Su R, Dong L, Li C, Nachtergaele S, et al. R-2HG exhibits anti-tumor activity by targeting FTO/m(6)A/MYC/CEBPA signaling. *Cell*. 2018;172(1-2):90–105.e23.
50 Wang X, Feng J, Xue Y, et al. Structural basis of N(6)-adenosine methylation by the METTL3-METTL14 complex. *Nature*. 2016;534 (7608):575–578.
51 Liu J, Yue Y, Han D, et al. A METTL3-METTL14 complex mediates mammalian nuclear RNA N6-adenosine methylation. *Nat Chem Biol*. 2014;10(2):93–95.
52 Jiang R, Dai Z, Wu J, Ji S, Sun Y, Yang W. METTL3 stabilizes HDAC5 mRNA in an m(6)A-dependent manner to facilitate malignant proliferation of osteosarcoma cells. *Cell Death Discov*. 2022;8 (1):179.
53 Liu H, Shu W, Liu T, Li Q, Gong M. Analysis of the function and mechanism of DIRAS1 in osteosarcoma. *Tissue Cell*. 2022;76: 101794.
54 Wang J, Wang W, Huang X, et al. m6A-dependent upregulation of TRAF6 by METTL3 is associated with metastatic osteosarcoma. *J Bone Oncol*. 2022;32:100411.
55 Zhou C, Zhang Z, Zhu X, et al. N6-Methyladenosine modification of the TRIM7 positively regulates tumorigenesis and chemoresistance in osteosarcoma through ubiquitination of BRMS1. *EBioMedicine*. 2020;59:102955.
56 Zhou X, Yang Y, Li Y, et al. METTL3 contributes to osteosarcoma progression by increasing DANCR mRNA stability via m6A modification. *Front Cell Dev Biol*. 2021;9:784719.
57 Li J, Rao B, Yang J, Liu L, et al. Dysregulated m6A-related regulators are associated with tumor metastasis and poor prognosis in osteosarcoma. *Front Oncol*. 2020;10:769.
58 Liu Z, Liu N, Huang Z, Wang W. METTL14 overexpression promotes osteosarcoma cell apoptosis and slows tumor progression via caspase 3 activation. *Cancer Manag Res*. 2020;12: 12759–12767.
59 Lu R, Wang P, Parton T, et al. Epigenetic perturbations by Arg882-mutated DNMT3A potentiate aberrant stem cell gene-expression program and acute leukemia development. *Cancer Cell*. 2016;30 (1):92–107.
60 Siddikuzzaman CG, Grace VMB. All trans retinoic acid and cancer. *Immunopharmacol Immunotoxicol*. 2011;33(2):241–249.
61 Stahl M, Tallman MS. Acute promyelocytic leukemia (APL): remaining challenges towards a cure for all. *Leuk Lymphoma*. 2019;60(13):3107–3115.
62 von Mehren M, Kane JM, Bui MM, et al. NCCN guidelines insights: soft tissue sarcoma, version 1.2021. *J Natl Compr Canc Netw*. 2020;18(12):1604–1612.